International Journal of Heat and Technology
Vol. 40, No. 4, August, 2022, pp. 939-946
Journal homepage: http://iieta.org/journals/ijht

Performance of Concrete Structure after Fire Disaster Based on Thermal Stress Coupling Field Analysis

Jingbo An*, Chunhong Wang, Yali Xu, Lei Zhu

Academy of City Construction and Transportation, Hefei University, Hefei 230601, China

Corresponding Author Email: ajbwch@hfuu.edu.cn

https://doi.org/10.18280/ijht.400410

Received: 20 May 2022
Accepted: 8 August 2022

Keywords:
thermal stress coupling field, fire disaster, concrete structure, strain analysis, stress analysis

ABSTRACT

Concrete is a kind of non-combustible material, but its mechanical properties are quite sensitive to temperature, once the temperature exceeds the limit temperature of steel and concrete, the structure of the building will be broken, therefore it's an urgent task to study the fire resistance, bearing capacity and stability of the concrete structure after fire disaster, and to respond to these questions, this paper studied the performance of concrete structure after fire disaster based on thermal stress coupling field analysis. At first, this paper gave the method for collecting displacement changes of each surface of concrete structure under high temperature during the experiment, and analyzed the thermal expansion strain of the concrete under thermal stress coupling effect. Then, to investigate the changes in the stability of concrete structure under high temperature, this paper simulated the thermal stress coupling of concrete structure after fire. After that, parameters of the concrete structure under high temperature were selected to further simulate the fire disaster temperature field of the concrete structure under high temperature and construct the corresponding heat conduction differential equations of the structure. At last, this paper analyzed the experimental results, proposed conclusions, and verified the effectiveness of the proposed parameter calculation method.

1. INTRODUCTION

For most of the large public buildings and special industrial structures, the key parts are generally built using new-type structures made of steel and concrete [1-9]. Although concrete structures have good corrosion resistance and durability, they are a kind of non-combustible material, and their mechanical properties are quite sensitive to temperature [10-16]. Since concrete structure buildings are prone to fire disaster with fast temperature rise and heavy smoke accumulation, once the temperature exceeds the limit temperature of steel and concrete, the structure of the building will be broken, and the bearing capacity and safety performance of the rest parts will be irreversibly weakened, thereby making the overall structure of the building be easily damaged or even collapse in severe cases [17-21]. Thus, it's an urgent task for field researchers to study the fire resistance, bearing capacity and stability of the concrete structure after fire disaster.

Kodur [22] proposed that now high-strength concrete is being widely used in many buildings, and structural fire safety is one of the primary design considerations. The author introduced the key features of the performance of high-strength concrete members under fire conditions, then according to the published data, the observation results, and the behavior trends of high-strength concrete members, they proposed a few creative strategies for reducing spalling and improving the fire resistance of the high-strength concrete structure members. Shallal and Aqil Mousa [23] researched the effect of direct fire on the shear transfer strength of concrete with several parameters taken into consideration, including concrete strength, number of stirrup legs, and fire duration. The experiment tested two groups of concrete samples with different strengths, each including 2 or 4 stirrup leg samples subjected to direct fire from one side, and the comparison results revealed the importance of using high-performance concrete (instead of increasing the number of stirrup legs) to cope with shear stress for the sake of safety, and an obvious decline in shear strength caused by the deterioration of the concrete cover after subjected to direct fire for 3 hours. Maciąg and Spodzieja [24] adopted the isotherm 500 method to calculate the bearing capacity of reinforced concrete slabs with a thickness larger than 15cm, and analyzed the support and span zone of the designed members, their research provided tables for designers, based on which slabs of demanded fire capacity could be designed.

Ahmad et al. [25] studied the effect of temperature rise on shear transfer capacity of reinforced concrete, they casted push-off samples using normal strength concrete, after curing, the samples were heated to 250℃ and 500℃ in an electric furnace, then a universal testing machine was adopted to test the shear transfer capacity of the cooled samples. Their research showed that, when the samples were heated to 250℃ and 500℃, the shear transfer capacity and stiffness were reduced, and the load level for the initiation of crack slip decreased as the temperature was increased. Malik et al. [26] pointed out that in fire incidents, different parts of the structure are subjected to uneven temperatures and consequently suffer un-uniform damage, they proposed a material-porosity-based approach to evaluate the reserved compressive strength by letting different parts of the high strength concrete structure to a range of rising temperatures. Then they used another set of the same samples and four techniques to determine the

aporosity, according to observation results, the relationship between temperature, strength, and porosity of normal and high strength concrete was figured out, the method and expressions suggested in this paper could be applied in predictions of the reserved strength and temperature field of members of the structure based on the assessed porosity of the concrete.

After reviewing existing literatures, it's found that current studies generally paid more attention to the high temperature bearing capacity of concrete structures in the event of a building fire. Field scholars have conducted series of tests on mechanical properties based on indoor experiments, and constructed strength criteria and constitutive relationships of concrete at room temperature and high temperature, and their research findings provided basis for subsequent studies. For the mechanical properties of concrete under high temperature, the effects of Poisson's ratio, density, thermal expansion coefficient, compressive strength, mix ratio, and size of the raw materials had been examined, but the studies on the real-time properties of concrete structures under high temperature during fire are insufficient, therefore, this paper studied the performance of concrete structure after fire disaster based on thermal stress coupling field analysis. In the second chapter, this paper gave the method for collecting displacement changes of each surface of concrete structure under high temperature during the experiment, and analyzed the thermal expansion strain of the concrete under thermal stress coupling effect. The third chapter simulated the thermal stress coupling of concrete structure after fire to investigate the changes in the stability of concrete structure under high temperature. In the fourth chapter, this paper selected parameters of concrete structure under high temperature for calculation and analysis to further simulate the fire disaster temperature field of the concrete structure under high temperature and construct the corresponding heat conduction differential equations of the structure. At last, this paper analyzed the experimental results, proposed conclusions, and verified the effectiveness of the proposed parameter calculation methods.

2. THERMAL EXPANSION STRAIN OF CONCRETE UNDER THERMAL STRESS COUPLING

After fire disaster, the temperature of concrete will rise rapidly, and the physical and chemical properties of concrete material will change accordingly. Temperature change can cause thermal expansion and contraction in concrete, and the uneven expansion of concrete structure in different directions will make its internal structure to produce continuous thermal stress, and the micro cracks inside the structure will expand and extend constantly under the continuous action of thermal stress, which can further cause temperature damage to the concrete structure and alter its shape and mechanical performance.

During the test, pressure was applied on the concrete structure with gradually rising temperature from three directions, throughout the temperature rising process, the size of the pressure was kept constant. In the test process, the temperature was increased until the preset maximum temperature, and the whole process lasted for 2 hours. The displacement changes of each surface of the concrete structure under high temperature were collected during the test. Figure 1, Figure 2, and Figure 3 respectively give the distribution of temperature measurement points on the concrete structure, the distribution of strain measurement points on the concrete structure, and the distribution of longitudinal temperature measurement points on the concrete beam.

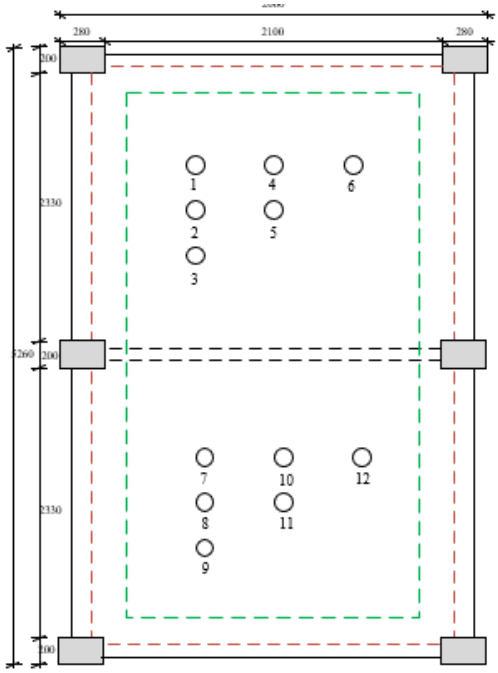

Figure 1. Distribution of temperature measurement points on the concrete structure

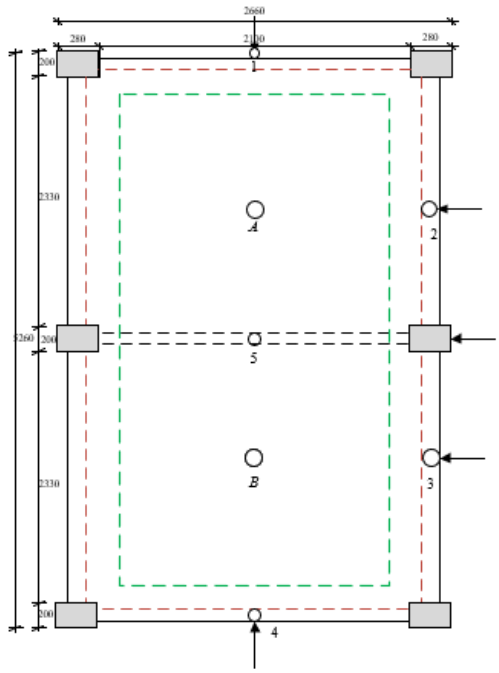

Figure 2. Distribution of strain measurement points on the concrete structure

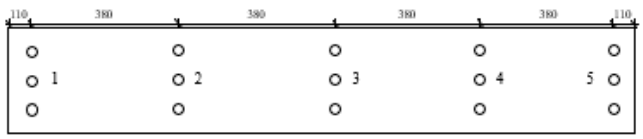

Figure 3. Distribution of longitudinal temperature measurement points on concrete beam

Assuming: $\rho_m(E)$ represents the tri-directional thermal strain of the high-temperature concrete structure under thermal stress coupling effect; $\rho_1(E)$ represents the axial thermal strain of the high-temperature concrete structure under thermal stress coupling effect; $\rho_2(E)$ represents the lateral thermal strain of the high-temperature concrete structure under thermal stress coupling effect; $\rho_3(E)$ represents the elevational thermal strain of the high-temperature concrete structure under thermal stress coupling effect; $SQ_{m,0}$ represents the initial tri-directional length of the high-temperature concrete structure; $SQ_{m,E}$ represents the tri-directional thermal expansion of the high-temperature concrete structure when it's heated to temperature E under three-dimensional stress; $SQ_{m,r}$ represents the tri-directional thermal expansion of the fine quartz sand sample when it's heated to temperature E under three-dimensional stress, then, based on the collected values of displacement changes of each surface of the concrete structure, the tri-directional thermal expansion of the high-temperature concrete structure under the thermal stress coupling effect can be calculated as follows:

$$\rho_m(E)=\frac{SQ_{m,E}-SQ_{m,r}}{SQ_{m,0}}(m=1,2,3) \tag{1}$$

Concrete is a kind of heterogeneous multi-phase composite material, when high-temperature concrete structure undergoes thermal expansion, the heterogeneous in each direction will cause certain differences in the amount of expansion in each direction, and result in unbalanced combined stress. Assuming: $\rho_m(E)$ represents the tri-directional thermal strain of the high-temperature concrete structure under thermal stress coupling effect and m=1, 2, 3; $\rho_D(E)$ represents the average tri-directional thermal expansion strain of the high-temperature concrete structure under thermal stress coupling effect; $\beta_D(E)$ represents the average tri-directional thermal expansion coefficient of the high-temperature concrete structure under thermal stress coupling effect; ΔE represents the temperature change of the test sample, then the following formula calculates the average tri-directional thermal expansion coefficient of the high-temperature concrete structure under thermal stress coupling effect:

$$R_D(E)=\frac{\rho_1(E)+\rho_2(E)+\rho_3(E)}{3} \tag{2}$$

$$\beta_D(E)=\frac{\rho_D(E)}{\Delta E} \tag{3}$$

Assuming: $\varphi_{m,E}$ represents the tri-directional thermal expansion stress of the high-temperature concrete structure under thermal stress coupling effect measured during the tests; $\varphi_{m,r}$ represents the tri-directional stress generated by the structure under the condition that the stresses in the three dimensions are the same; MO_R represents the elastic modulus of the structure; $\rho_{m,R}$ represents the tri-directional thermal expansion strain of the structure under thermal stress coupling effect measured during the tests; in order to improve the calculation accuracy of displacement and stress, in this paper, $\rho_m(E)$ was set to be equivalent to the difference between $\varphi_{m,E}$ and $\varphi_{m,r}$, then the formula below calculates the actual tri-directional thermal expansion stress of the high-temperature concrete structure under thermal stress coupling effect:

$$\varphi_m(E)=\varphi_{m,E}-\varphi_{m,r}=\varphi_{m,E}-MO_R\rho_{m,r}(m=1,2,3) \tag{4}$$

This paper divided the development process of micro cracks and structural performance changes of concrete structure after fire into five stages: compacted stage, elastic stage, stable crack development stage, unstable crack development stage, and post-peak failure stage. Assuming: φ_1 represents the maximum principal stress of the concrete structure sample under thermal stress coupling effect; φ_3 represents the minimum principal stress; NJ represents the cohesive force of the concrete material; ψ represents the internal friction angle of rock and soil materials, then the strength parameters of the concrete structure in the above stages can be described by the Mohr-Coulomb criterion of rock failure:

$$G=\frac{1}{2}(\varphi_1\cdot\varphi_3)+\frac{1}{2}(\varphi_1+\varphi_3)sin\,\psi-cos\,\psi=0 \tag{5}$$

According to the relationship between φ_3, φ_1-φ_3, and φ_1+φ_3, by combining the two formulas below, the parameters l_1, l_2, κ_1, and κ_2 could be attained:

$$\varphi_1-\varphi_3=l_1\varphi_3+\kappa_1 \tag{6}$$

$$\varphi_1+\varphi_3=l_2\varphi_3+\kappa_2 \tag{7}$$

By combining Formulas 5, 6, and 7, the correlations between NJ, ψ and (l_1, κ_1), (l_2, κ_2) could be attained as:

$$\psi=sin^{-1}\left(\frac{l_1}{l_2}\right) \tag{8}$$

$$NJ=\frac{1}{2\cos\psi}\kappa_1-\frac{l_1}{2l_2\cos\psi}\kappa_2 \tag{9}$$

3. SIMULATION OF THERMAL STRESS COUPLING OF CONCRETE STRUCTURE AFTER FIRE

Temperature damage and variations in the shape, structure, and mechanical properties are the main reasons for the damage of concrete structures after fire, at the same time, the thermal stress generated due to the unbalanced thermal expansion in different directions inside the high-temperature concrete also causes great changes to the bearing capacity of the concrete structure. In order to investigate the stability of high-temperature concrete structure after fire, it is necessary to carry out thermal stress coupling simulation and analysis on the concrete structure after fire.

The core reason causing stress and strain to the high-temperature concrete structure after fire is the temperature load and stress load generated due to the unbalanced thermal expansion. Default the temperature change interval of the micro-elements of high-temperature concrete structure after fire is [τ_1, τ_2], the amount of temperature change is τ=τ_1-τ_2, the thermal expansion coefficient is β, then the length change of \ micro-elements da, db, and dc of the structure in the three directions of a, b and c are respectively (1+$\beta\tau$)da, (1+$\beta\tau$)db, and (1+$\beta\tau$)dc, then the strain components satisfy:

$$\begin{cases}\rho_{a0}=\rho_{b0}=\rho_{c0}=\beta\tau\\ \alpha_{ab0}=\alpha_{bc0}=\alpha_{ca0}=0\end{cases} \tag{10}$$

However, under the constraints of structural and material properties, the micro-elements of the high-temperature concrete structure couldn't expand or contract casually, which is also the cause of thermal stress. In other words, the total strain of the micro-elements of the high-temperature concrete structure is generated by the joint actions of temperature and stress. Assuming: H represents the modulus of shear elasticity; NJ represents the modulus of elasticity; λ represents the Poisson's ratio; Ψ represents the volume stress, then, based on the Hooke's Law, there are:

$$\begin{cases}\rho_a=\dfrac{\partial v}{\partial a}=\dfrac{1}{MO}\left[\varphi_a-\lambda(\varphi_b+\varphi_c)\right]+\beta\tau\\ \rho_b=\dfrac{\partial v}{\partial b}=\dfrac{1}{MO}\left[\varphi_b-\lambda(\varphi_a+\varphi_c)\right]+\beta\tau\\ \rho_c=\dfrac{\partial v}{\partial c}=\dfrac{1}{MO}\left[\varphi_c-\lambda(\varphi_b+\varphi_a)\right]+\beta\tau\end{cases} \tag{11}$$

$$\alpha_{ab}=\frac{\phi_{ab}}{H},\alpha_{bc}=\frac{\phi_{bc}}{H},\alpha_{ca}=\frac{\phi_{ca}}{H} \tag{12}$$

$$H=NJ/2(1+\lambda) \tag{13}$$

$$\Psi=\varphi_a+\varphi_b+\varphi_c \tag{14}$$

By combining Formulas 11 and 14, the expression form based on the generalized Hooke's Law could be attained:

$$\begin{cases}\varphi_a=2H\rho_a+\dfrac{\lambda}{1+\lambda}\Psi-2H\beta\tau\\ \varphi_b=2H\rho_b+\dfrac{\lambda}{1+\lambda}\Psi-2H\beta\tau\\ \varphi_c=2H\rho_c+\dfrac{\lambda}{1+\lambda}\Psi-2H\beta\tau\end{cases} \tag{15}$$

The following formula calculates the volume strain:

$$t=\rho_a+\rho_b+\rho_c=\frac{1-2\lambda}{1+\lambda}\frac{\Psi}{2H}+3\beta\tau \tag{16}$$

In the meantime, there is:

$$\Psi=\frac{MO}{1-2\lambda}(t-3\beta\tau) \tag{17}$$

Assuming: γ represents the thermal stress parameter; by introducing the *lame* constant μ, there are:

$$\begin{cases}\varphi_a=2H\rho_a+\mu t-\gamma\tau\\ \varphi_b=2H\rho_b+\mu t-\gamma\tau\\ \varphi_c=2H\rho_c+\mu t-\gamma\tau\end{cases} \tag{18}$$

$$\gamma=\frac{\beta MO}{1-2\lambda}=\beta(3\mu+2H) \tag{19}$$

$$\mu=\frac{MO\lambda}{(1+\lambda)(1-2\lambda)} \tag{20}$$

Assuming: A, B, C represent the components of thermal stress on each axis, then, based on the elastic mechanics, equilibrium differential equations could be built for the micro-elements of the high-temperature concrete structure:

$$\begin{cases}\dfrac{\partial\varphi_a}{\partial a}+\dfrac{\partial\phi_{ba}}{\partial b}+\dfrac{\partial\phi_{ca}}{\partial c}+A=0\\ \dfrac{\partial\varphi_b}{\partial b}+\dfrac{\partial\phi_{cb}}{\partial c}+\dfrac{\partial\phi_{ab}}{\partial a}+B=0\\ \dfrac{\partial\varphi_c}{\partial c}+\dfrac{\partial\phi_{ac}}{\partial a}+\dfrac{\partial\phi_{bc}}{\partial a}+C=0\end{cases} \tag{21}$$

Based on above derivation process, the equilibrium differential equations of micro-elements of the high-temperature concrete structure in the three directions of a, b, and c can be attained further:

$$\begin{cases}(\mu+H)\dfrac{\partial\rho}{\partial a}+H\nabla^2 v-\gamma\dfrac{\partial\tau}{\partial a}+A=0\\ (\mu+H)\dfrac{\partial\rho}{\partial b}+H\nabla^2 v-\gamma\dfrac{\partial\tau}{\partial b}+B=0\\ (\mu+H)\dfrac{\partial\rho}{\partial c}+H\nabla^2 v-\gamma\dfrac{\partial\tau}{\partial c}+C=0\end{cases} \tag{22}$$

where, the Laplace operator is:

$$\nabla^2=\frac{\partial^2}{\partial a^2}+\frac{\partial^2}{\partial b^2}+\frac{\partial^2}{\partial c^2} \tag{23}$$

The corresponding partial differential equation attained based on the thermo-elasticity theory is given by the following formula:

$$\begin{aligned}\{\rho\}&=\{\rho_a,\rho_b\rho_c,\alpha_{ab},\alpha_{bc},\alpha_{ca}\}^T\\ &=\left\{\frac{\partial v}{\partial a},\frac{\partial u}{\partial b},\frac{\partial q}{\partial c},\frac{\partial u}{\partial a}+\frac{\partial v}{\partial b},\frac{\partial q}{\partial b}+\frac{\partial u}{\partial c},\frac{\partial v}{\partial c}+\frac{\partial q}{\partial a}\right\}^T\end{aligned} \tag{24}$$

Assuming: A^*, B^*, and C^* represent the components of surface stress of micro-elements at the boundaries of the structure; k, n, and m represent their cosine values in the normal direction, then the displacement components of the micro-elements of the structure are approximated:

$$\begin{cases}\dfrac{\partial^2\rho_a}{\partial b^2}+\dfrac{\partial^2\rho_b}{\partial a^2}=\dfrac{\partial^2\alpha_{ab}}{\partial a\partial b}\\ \dfrac{\partial^2\rho_b}{\partial c^2}+\dfrac{\partial^2\rho_c}{\partial b^2}=\dfrac{\partial^2\alpha_{bc}}{\partial b\partial c}\\ \dfrac{\partial^2\rho_c}{\partial a^2}+\dfrac{\partial^2\rho_a}{\partial c^2}=\dfrac{\partial^2\alpha_{ca}}{\partial c\partial a}\\ \dfrac{\partial^2\rho_c}{\partial a^2}+\dfrac{\partial^2\rho_a}{\partial c^2}=\dfrac{\partial^2\alpha_{ca}}{\partial c\partial a}\\ \dfrac{\partial}{\partial a}\left(\dfrac{\partial\alpha_{bc}}{\partial b}+\dfrac{\partial\alpha_{ca}}{\partial c}+\dfrac{\partial\alpha_{ab}}{\partial a}\right)=2\dfrac{\partial^2\rho_c}{\partial b\partial c}\\ \dfrac{\partial}{\partial b}\left(\dfrac{\partial\alpha_{ab}}{\partial c}+\dfrac{\partial\alpha_{bc}}{\partial a}+\dfrac{\partial\alpha_{ca}}{\partial b}\right)=2\dfrac{\partial^2\rho_b}{\partial c\partial a}\\ \dfrac{\partial}{\partial c}\left(\dfrac{\partial\alpha_{ab}}{\partial a}+\dfrac{\partial\alpha_{bc}}{\partial b}+\dfrac{\partial\alpha_{ca}}{\partial c}\right)=2\dfrac{\partial^2\rho_b}{\partial a\partial b}\end{cases} \tag{25}$$

The boundary conditions of the surface stress are:

$$\begin{cases} A^* = \varphi_a k + \phi_{ba} n + \phi_{ca} m \\ B^* = \varphi_b n + \phi_{cb} m + \phi_{ab} k \\ C^* = \varphi_c m + \phi_{ac} k + \phi_{bc} n \end{cases} \tag{26}$$

4. MODELING OF THE TEMPERATURE FIELD AND HEAT CONDUCTION OF THE HIGH-TEMPERATURE CONCRETE STRUCTURE

To analyze the coupling effect between temperature field and stress field of the high-temperature concrete structure, this paper selected a few parameters of the high-temperature concrete structure for calculation and analysis, including the elastic modulus, Poisson's ratio, density, thermal expansion coefficient, compressive strength, thermal conductivity, specific heat capacity, and the comprehensive heat exchange coefficient between hot smoke flow and the high-temperature concrete structure, then, the fire temperature field of the high-temperature concrete structure was simulated, and the corresponding structural heat conduction differential equation was constructed.

As for the siliceous aggregates material, this paper referred to the standards given by the European codes, then the thermal conductivity of the high-temperature concrete structure could be calculated as:

$$\mu = 2 - 0.25\frac{E}{120} + 0.014\left(\frac{E}{120}\right)^2 \quad \left(25^\circ C \le E \le 1000^\circ C\right) \tag{27}$$

The formula for calculating the specific heat capacity of the high-temperature concrete structure is:

$$d_d = 852 + 82\left(\frac{E}{110}\right) - 3.8\left(\frac{E}{110}\right)^2 \quad \left(0^\circ C \le E \le 1000^\circ C\right) \tag{28}$$

The comprehensive heat exchange coefficient between the hot smoke flow and the high-temperature concrete structure can be calculated by the formula below:

$$f_g = 7 \times o^{\left(\frac{E}{37000}\right)} + 0.85 \tag{29}$$

Assuming: *TE* represents the temperature at time moment *e*; *e* represents time; E_0 represents the initial temperature; β and γ are curve parameters, then the fire temperature field of the simulated high-temperature concrete structure can be described by a fire temperature curve with adjustable parameters given by the following formula:

$$E = E_0 + X \times \left(1 - 0.325 \times t^{\beta\tau} - 0.675 \times t^{\gamma\tau}\right) \tag{30}$$

This paper defaults that the heat transfer of high-temperature concrete structure during fire disaster is mainly carried out in the form of heat conduction. The following formula gives the basic differential equation for the transient heat conduction of high-temperature concrete structure:

$$\frac{\partial E}{\partial e} = \frac{1}{d\sigma}\left[\begin{array}{l} \frac{\partial}{\partial a}\left(\mu\frac{\partial E}{\partial a}\right) + \frac{\partial}{\partial b}\left(\mu\frac{\partial E}{\partial b}\right) \\ + \frac{\partial}{\partial c}\left(\mu\frac{\partial E}{\partial c}\right) \end{array}\right] + \frac{1}{d\sigma} w_c \tag{31}$$

If the heat is transferred along the direction of the thickness of the cross section of the high-temperature concrete structure during fire, then the above formula was subjected the conversion in the form of one-dimensional temperature transfer field shown by the formula below:

$$\frac{\partial E}{\partial e} = \frac{1}{d\sigma}\left[\frac{\partial}{\partial a}\left(\mu\frac{\partial E}{\partial a}\right)\right] \tag{32}$$

5. EXPERIMENTAL RESULTS AND ANALYSIS

Figure 4 and Table 1 give the load and temperature values corresponding to the load and peak strain of nodes in the middle part of the concrete structure sample. According to the figure and the table, during the simulation test, the higher the fire temperature, the faster it takes for the strain of the concrete structure sample to reach the peak value. But when the strain of the concrete structure sample reached the peak value, the load of the concrete structure sample didn't decrease within 1h, then in the later stage, it decreased continuously with the rise of temperature, indicating that the high temperature concrete structure sample maintained a good corresponding relationship with the load during the process of continuous strength decrease.

In test H1, the high-temperature was applied for about 1h, the concrete structure sample suffered serious damage, such as large deflection deformation, tearing and cracking, blocky structure spalling and partial or complete detaching of steel bars. Table 2 shows the cracking situations at 15 positions in test H1, wherein the lateral crack position was numbered 9, and the points touching the fire traversed the entire concrete structure sample. Positions 1 and 2 were multi-directional cracks of the concrete structure sample developed from vertical cracks; positions 7,10,11,12 were vertical cracks developed to intersect with multi-directional cracks; position 3 was vertical crack developed from the lateral crack of position 9. The diagonal cracks didn't run through the entire concrete structure sample, and the specific length data are shown in Table 2.

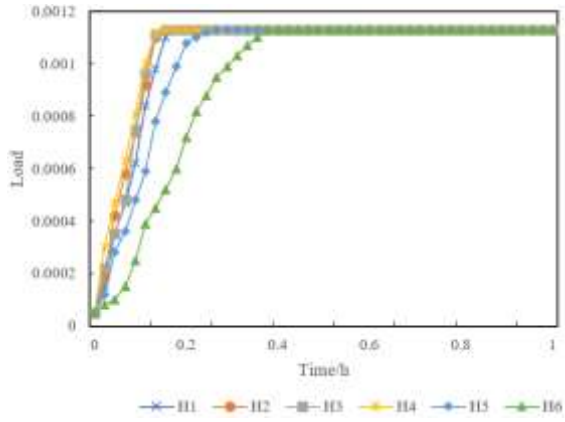

Figure 4. The load change of nodes in the middle part of the concrete structure sample

Table 1. Load and temperature corresponding to peak strain of the concrete structure sample

Test No.	Load peak	Time peak	Temperature peak
H1	65.241	3629	116
H2	63.629	1847	284
H3	62.517	1162	257
H4	58.592	795	369
H5	45.629	718	384
H6	16.327	692	349

Table 2. The cracking of concrete structure sample in test H1

Crack position No.	Crack direction	Crack angle	Crack length
1	Multi-directional	/	52
2	Multi-directional	/	69
3	Vertical	/	40
4	Diagonal	Clockwise 35º	48
5	Diagonal	Clockwise 35º	56
6	Diagonal	Clockwise 50º	22
7	Vertical	/	8
8	Diagonal	Clockwise 45º	13
9	Lateral	/	5
10	Vertical	/	13
11	Vertical		11
12	Vertical	/	251
13	Diagonal	Clockwise 60º	48
14	Diagonal	Clockwise 60º	36
15	Diagonal	Clockwise 35º	22

The average temperature of each cross section of the concrete structure sample was compared with the temperature rise curve of the firing point, the average temperature of different cross sections of the concrete structure sample is shown in Figure 5. As can be seen from the figure, the average temperature of different cross sections showed a step-shaped pattern, meaning that the larger the length of the concrete structure sample, the lower the temperature.

Figure 6 shows the strain change of the concrete beam in test H4. According to the figure, by comparing with the limiting tensile strain of the concrete beam under normal temperature, after the fire disaster, the maximum strain of the tensile zone of the beam exceeded 500, with an increment of 400 units. It can be considered that the concrete beam cracked after 0.5h during the fire disaster, and all measurement points of H4-J1, H4-J2, H4-J3 and H4-J4 were under pressure, indicating that during test H4, the limiting compressive strain of the concrete structure sample decreased greatly during fire.

Figure 7 shows the stress-load curves of supporting nodes at the bottom of the concrete structure sample. At room temperature, the bottom of the concrete structure sample was the main load bearer. During fire disaster, the bearing capacity of the sample bottom was lost gradually. According to the figure, with the temperature rise of the firing point, the stress zone of the sample gradually spread to both sides and then concentrated at the waist of both ends, then, with the progress of the test, it developed and extended to the entire sample.

The load changes of the bottom of the HD concrete structure sample under shear force and bending force are given in Figure 8. According to the figure, when the load reached more than 1000kN, the bottom of the concrete structure sample was damaged by shear, and this is basically consistent with the test phenomenon. Figure 9 compares the calculation results of the shear bearing capacity of design specification standard, the reference method based on finite elements, and the proposed method, as can be seen from the figure, the value of shear bearing capacity calculated by the proposed method was basically the same with the theoretical value. The calculation results of the limiting bearing capacity of the concrete structure at high temperature are listed in Table 3, which had further verified the effectiveness of the proposed method.

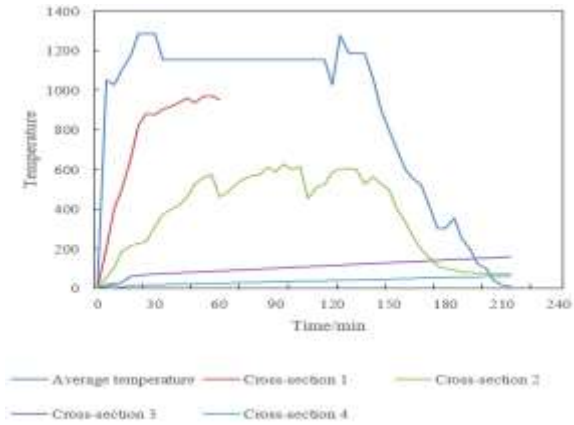

Figure 5. The change of average temperature of different cross sections

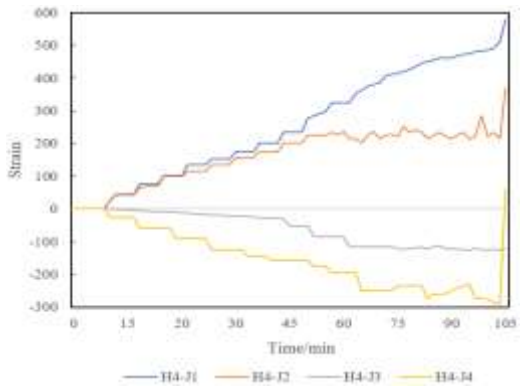

Figure 6. Strain change of concrete beam in test H4

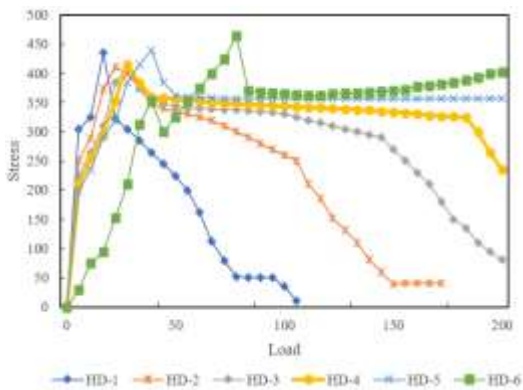

Figure 7. Stress-load curves of supporting nodes at the bottom of the concrete structure sample

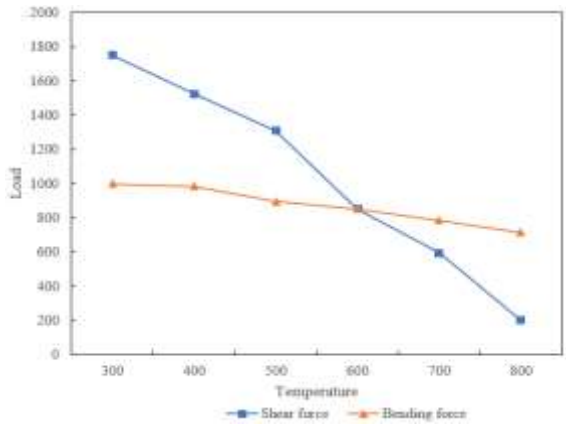

Figure 8. Load change under shear force and bending force

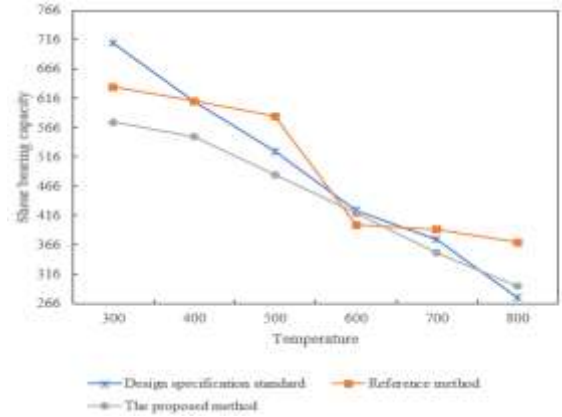

Figure 9. Shear bearing capacity calculated by different methods

Table 3. Calculation results of limiting bearing capacity of concrete structure at high temperature

Temperature	Design specification standard		Reference method	The proposed method	
	Shear force	Bending force		Shear force	Bending force
300	514.96	829.63	659.27	592.61	/
400	417.28	728.51	527.41	584.37	/
500	403.62	516.38	418.29	518.25	/
600	364.58	372.42	328.61	326.59	392.67
700	248.63	296.38	311.27	348.26	258.19
800	259.11	128.37	395.62	342.17	200.52
900-1200	/	2.68σ (T_d,t)	/	/	/

6. CONCLUSION

This paper studied the performance of concrete structure after fire based on thermal stress coupling field analysis. At first, it gave the method for collecting displacement changes of each surface of concrete structure under high temperature during the experiment, and analyzed the thermal expansion strain of the concrete under thermal stress coupling effect. Then, to investigate the changes in the stability of concrete structure under high temperature, this paper simulated the thermal stress coupling of concrete structure after fire. After that, parameters of the concrete structure under high temperature were selected to further simulate the fire disaster temperature field of the concrete structure under high temperature and construct the corresponding heat conduction differential equations of the structure. Combining with tests, this paper counted the load and temperature values corresponding to the load and peak strain of nodes in the middle part of the concrete structure sample, gave the cracking situations of the concrete structure sample, compared the average temperature of each cross section of the concrete structure sample with the temperature rise curve of the firing point, plotted the stress-load curves of supporting nodes at the bottom of the concrete structure sample, and gave the corresponding analysis results. At last, this paper calculated the limiting bearing capacity of concrete structure at high temperature, and further verified the effectiveness of the proposed algorithm.

REFERENCES

[1] Zade, N.P., Bhosale, A., Sarkar, P., Davis, R. (2022). In-plane seismic response of autoclaved aerated concrete block masonry-infilled reinforced concrete frame building. ACI Structural Journal, 119(2): 45-60.

[2] Oyebisi, S., Ede, A., Olutoge, F., Ofuyatan, O., Alayande, T. (2019). Building a sustainable world: Economy index of geopolymer concrete, 10th Int. In Struct. Eng. Constr. Conf. (ISEC-10).

[3] Secer, M., Arslan, T. (2018). Effects of construction sequence on reinforced concrete building analysis. In International Conference on Numerical Modelling in Engineering, pp. 123-134. https://doi.org/10.1007/978-981-13-2405-5_10

[4] Bennai, F., Ferroukhi, M.Y., Benmahiddine, F., Belarbi, R., Nouviaire, A. (2022). Assessment of hygrothermal performance of hemp concrete compared to conventional building materials at overall building scale. Construction and Building Materials, 316: 126007. https://doi.org/10.1016/j.conbuildmat.2021.126007

[5] Salesa, Á., Esteban, L. M., Lopez-Julian, P.L., Pérez-Benedicto, J.Á., Acero-Oliete, A., Pons-Ruiz, A. (2022). Evaluation of characteristics and building applications of multi-recycled concrete aggregates from precast concrete rejects. Materials, 15(16): 5714. https://doi.org/10.3390/ma15165714

[6] Geng, Z. (2022). Optimization of prefabricated concrete frame building based on genetic algorithm. In International Conference on Multi-modal Information Analytics, pp. 145-153. https://doi.org/10.1007/978-3-031-05484-6_18

[7] Zhang, X., Xuan, L., Huang, W., Yuan, L., Li, P. (2022). Structural design and analysis for a timber-concrete hybrid building. Advanced Concretes and Their Structural Applications. https://doi.org/10.3389/fmats.2022.844398

[8] Varlamov, A.A., Rimshin, V.I., Norec, A.I., Davydova,

A.M. (2019). Building model of behaviour of concrete under load. In IOP Conference Series: Materials Science and Engineering, 661(1): 012074. https://doi.org/10.1088/1757-899X/661/1/012074
[9] Widarda, D.R., Hidajat, M.Y. (2019). Application of Self Mass Damper in multi-story concrete building. In MATEC Web of Conferences, 258: 05006. https://doi.org/10.1051/matecconf/201925805006
[10] Canbaz, M., Dakman, H., Arslan, B., Büyüksungur, A. (2019). The effect of high-temperature on foamed concrete. Computers and Concrete, An International Journal, 24(1): 1-6. https://doi.org/10.12989/cac.2019.24.1.001
[11] Venkateswara Rao, A., Srinivasa Rao, K. (2018). Effect of temperature on fly ash concrete. Indian Concrete Journal, 92(8): 59-64.
[12] Makeeva, A., Amelina, A., Semenov, K., Barabanshchikov, Y. (2018). Temperature action in analysis of thermal stressed state of massive concrete and reinforced concrete structures. In MATEC Web of Conferences, 245: 03016. https://doi.org/10.1051/matecconf/201824503016
[13] Huang, B., Zhang, Y., Qi, T., Han, H. (2018). Static and dynamic properties and temperature sensitivity of emulsified asphalt concrete. Advances in Materials Science and Engineering. https://doi.org/10.1155/2018/7067608
[14] Aziz, Y.H.A., Zaher, Y.A., Wahab, M.A., Khalaf, M. (2019). Predicting temperature rise in Jacketed concrete beams subjected to elevated temperatures. Construction and Building Materials, 227: 116460. https://doi.org/10.1016/j.conbuildmat.2019.07.186
[15] Fedorov, V.S., Levitsky, V.E. (2018). Modeling of concrete thermal power resistance during the high-temperature heating. In IOP Conference Series: Materials Science and Engineering, 456(1): 012041. https://doi.org/10.1088/1757-899X/456/1/012041
[16] Hagedorn, R., Martí-Vargas, J.R., Dang, C.N., Hale, W.M., Floyd, R.W. (2019). Temperature gradients in bridge concrete I-girders under heat wave. Journal of Bridge Engineering, 24(8): 04019077. https://doi.org/10.1061/(ASCE)BE.1943-5592.0001454
[17] Aniskin, N., Nguyen, T.C. (2019). Influence factors on the temperature field in a mass concrete. In E3S Web of Conferences, 97: 05021. https://doi.org/10.1051/e3sconf/20199705021
[18] Rozsypalová, I., Frantík, P., Vyhlídal, M., Šimonová, H., Daněk, P., Karel, O., Keršner, Z. (2018). Mechanical fracture parameters of concrete exposed to high temperatures related to approximation of temperature fields in experimental panels. In Proceedings for the 2018 fib Congress held in Melbourne, Switzerland, 670: 671.
[19] Demirel, B., Gultekin, E., Alyamac, K.E. (2019). Performance of structural lightweight concrete containing metakaolin after elevated temperature. KSCE Journal of Civil Engineering, 23(7): 2997-3004. https://doi.org/10.1007/s12205-019-1192-x
[20] Chen, Y.Y. (2019). Effects observed in temperature rise evaluation tests for mass concrete. Journal of Technology, 34(2): 81-94.
[21] Derui, H., Wei, J., Kuizhou, L., Yujie, S., Zhonghua, H., Yang, L.I. (2019). GFRP reinforced concrete adhesion in low temperature environment. In IOP Conference Series: Earth and Environmental Science, 304(5): 052028. https://doi.org/10.12989/cac.2019.24.1.001
[22] Kodur, V.K. (2018). Innovative strategies for enhancing fire performance of high-strength concrete structures. Advances in Structural Engineering, 21(11): 1723-1732. https://doi.org/10.1177/1369433218754335
[23] Shallal, M.A., Al Musawi, A.M.K. (2018). Tests of residual shear transfer strength of concrete exposed to fire. Archives of Civil Engineering, 64(2): 187-199. https://doi.org/10.2478/ace-2018-0024
[24] Maciąg, M., Spodzieja, S. (2018). Designing reinforced concrete slabs under fire condition. In MATEC Web of Conferences, 196: 02036. https://doi.org/10.1051/matecconf/201819602036
[25] Ahmad, S., Bhargava, P., Chourasia, A. (2018). Shear transfer capacity of reinforced concrete exposed to fire. In IOP Conference Series: Earth and Environmental Science, 140(1): 012146. https://doi.org/10.1088/1755-1315/140/1/012146
[26] Malik, M., Bhattacharyya, S.K., Barai, S.V. (2022). Temperature, porosity and strength relationship for fire affected concrete. Materials and Structures, 55(2): 1-18. https://doi.org/10.1617/s11527-022-01898-9